International Journal of GEOMATE, Oct., 2021, Vol.21, Issue 86, pp.147-158
ISSN: 2186-2982 (P), 2186-2990 (O), Japan, DOI: https://doi.org/10.21660/2021.86.j2304
Geotechnique, Construction Materials and Environment

ESTIMATING LIQUEFACTION RESISTANCE IMPROVEMENT DUE TO STONE COLUMNS FROM QUALITY CONTROL TESTS

Adham Gamal Diaaeldin Abdelrazek[1], *Sherif Adel Yahia Akl [1]

[1] Soil Mechanics and Foundations Research Laboratory, Cairo University, Egypt;

*Corresponding Author, Received: 30 Aug. 2021, Revised: 24 Sept. 2021, Accepted:03 Oct. 2021

ABSTRACT: Stone columns are often used in cohesionless soils to decrease their liquefaction susceptibility; however, methods of predicting how much liquefaction resistance increases due to stone columns greatly vary. All these methods depend on knowing the stone column stiffness but the quality control tests in the field do not lead to measuring actual column stiffness directly, especially the popular plate load tests on a single stone column. A series of axisymmetric numerical simulations of stone column compression investigate the relationship between the actual stone column stiffness and that interpreted from test results. The paper also presents the results of plane-strain numerical models simulating a reference earthquake acting on a unit cell improved by a stone column. The dynamic analysis assesses the change in liquefaction resistance with increasing column stiffness and friction angle. The analysis results show that the PM4Sand dynamic constitutive model is more suitable than the UBC3D-PLM model in capturing the sensitivity of liquefaction resistance to soil improvement and stone column stiffness. The degrees of improvement in liquefaction resistance predicted in the study agree well with what the theories based on combined shear and flexural stone column deformation mechanisms predict. Finally, the paper presents design curves to get a quick estimate of the degree of improvement in liquefaction resistance from plate load test results.

Keywords: Stone columns; Plate load tests; Liquefaction Resistance; Dynamic analysis; Dynamic constitutive model

1. INTRODUCTION

Vibro-replacement or constructing stone columns is a traditional method of improving soft clays to withstand loads from structures such as embankments and airports [1-3]. They are also used to improve the liquefaction resistance of loose sandy soils by densifying surrounding soil during construction and providing lateral confinement [4]. The stone columns carry a significant portion of the total load (both static and dynamic); hence, reinforcing the soil medium. Stone columns also reduce excess pore water pressures in the soil by providing a drainage path (due to stone columns' large relative permeability). In projects with an abundance of silty sand soil deposits, vibro-replacement is often recommended to improve liquefaction resistance even if the settlements are acceptable in static conditions. The use of stone columns to mitigate liquefaction has been reported in many projects such as the wastewater treatment plant of Santa Barbara in California, USA; and the oil storage tanks on the Black Sea coast in Georgia [5]. The stone columns design process has been ubiquitously described in the literature [5-7]. These methods depend on the knowledge of stone column stiffness and its ratio to native soil stiffness.

Verification of stone column design stiffness and shear strength parameters in the site is indispensable in any professional project. There are various types of quality control methods such as: field tests after stone column construction (cone penetration and standard penetration tests), unit cell or stone column loading. The simplest and most common method of quality control is the in-situ plate load tests (PLT) on a single stone column. However, there is no direct relationship between the stiffness value interpreted from the plate load test (PLT) results and the actual stiffness of the stone column on site. Hence, the degree of enhancement in liquefaction resistance from the stone columns is not indicated by the common quality control tests in the field. This issue is further complicated by the wide variation in empirical methods used to estimate the enhancement in liquefaction resistance [6, 8-11].

The paper presents two sets of finite element analyses to investigate the interplay between stone columns and native soils under static and dynamic loads. The first set simulates a static plate loading applied to a single column to clarify the ambiguous relation between interpreted and actual column stiffness. The second set examines a unit cell behavior under typical earthquake application and calculates improvement in liquefaction resistance. Results from the second set are used to evaluate existing dynamic constitutive models and the empirical methods of estimating the degree of

liquefaction resistance. This paper aims to produce a series of curves to relate the plate load test results (load vs. settlement curves) to the cyclic shear stress reduction factor (K_G). This relationship enables the quality control engineer to perform a preliminary assessment of the column's effectiveness on site.

2. BACKGROUND STUDY

Liquefaction occurs due to rapid cyclic loading because it leads to soil compaction and generates excess pore water pressure which decreases the soil's effective stress. When effective stress tends to reach a zero value, the granular soil material transforms into a liquefied state. Two earthquakes have occurred; in Alaska, USA, and Niigata, Japan, in 1964, resulted in significant liquefaction related damages and alerted the geotechnical community to the importance of studying this phenomenon and the different methods of its mitigation [12]. Stone columns improve liquefaction resistance by sustaining a considerable amount of shear stresses compared to the surrounding loose sandy soils due to its higher shear strength. This difference in shear strength redistributes the induced shear stresses and increases resistance to soil liquefaction.

The degree of improvement in liquefaction resistance is the ratio between shear stresses without the stone column, and the shear stresses with stone columns. This ratio is the reduction in cyclic shear stress as a result of the stone column rigidity, and it is represented by the shear stress reduction factor (K_G) [8-11]. The current design procedures [6, 8] assume shear strain compatibility between liquefiable soil and stiff column material and that shear stresses are proportional to shear stiffness of the material. This method uses Eqs. 1-3 to calculate the degree of improvement.

$$\tau_s = \frac{1}{G_r}\tau_{sc} \quad (1)$$

$$\tau_{sc} = \frac{\tau}{A_r + \frac{1}{G_r}(1-A_r)} \quad (2)$$

$$K_G = \frac{\tau_S}{\tau} \quad (3)$$

In the equations above, τ_s is the cyclic shear stress in the soil, τ_{sc} is the cyclic shear stress in the stone column, τ is the cyclic shear stress (CSR) calculated using the simplified procedure proposed by Seed and Idriss [12]. The shear modulus ratio, G_r, is the ratio between the stone column (G_{sc}) and soil shear modulus (G_S), and A_r is the area replacement ratio.

On the other hand, Goughnour and Pestana [9] assume that stone columns adopt a flexural beam behavior due to their slenderness ratio. As a result, tensile stresses occur in the outer portion of the cross-section and compressive stresses occur near the center. Hence, the stone columns carry no additional shear stresses, and the degree of improvement is calculated using Eqs. 4 and 5.

$$K_G = \frac{1+A_r(n-1)}{1+A_r(G_r-1)} \quad (4)$$

$$n = G_r \frac{\left(\frac{1-\nu_{sc}}{1-2\nu_{sc}}\right)}{\left(\frac{1-\nu_s}{1-2\nu_s}\right)} \quad (5)$$

The terms in the equations above are A_r is the area replacement ratio, n is the vertical stress ratio, ν_{sc} is the stone column Poisson's ratio, and ν_s is the soil Poisson's ratio. Preibe [5] assumes that the shear stresses are proportionally distributed between soil and stone columns in the same way as the distribution of static loads. The degree of cyclic shear stress reduction is assumed to be the reciprocal of the improvement factor.

$$K_G = \alpha = \frac{1}{n_0} = \frac{K_{aC}\left(1-\frac{A_c}{A}\right)}{\frac{A_c}{A}+K_{aC}\left(1-\frac{A_c}{A}\right)^2} \quad (6)$$

In Eq. 6, α is the shear stress reduction factor, n_0 is the improvement factor, K_{aC} is the stone column active earth pressure, A is the attributable area within the compaction grid (unit cell), and A_C is the cross-section area of the stone column.

Recent studies [10,11,13-15] suggest that the stone column deformation is a combination of flexural and shear modes. Hence, the stone columns are far less effective in reducing shear stresses in surrounding soils than predicted by the shear strain compatibility theory. Also, this type of deformation leads to lower K_G results than assuming flexural deformation only, making the Goughnour and Pestana [9] approach the most conservative one.

Rayamajhi et al. [11] proposed a modified equation to estimate the shear stress reduction factor as shown in Eqs. 7 and 8. This modification accounts for both, flexural deformations and shear strain compatibility behavior between the columns and surrounding soil.

$$K_G = \frac{1}{G_r[A_r\gamma_r + \frac{1}{G_r}(1-A_r)]} \leq 1 \quad (7)$$

$$\gamma_r = 1.04(G_r)^{-0.65} - 0.04 \leq 1 \quad (8)$$

In the equations above, γ_r is the ratio of shear strain in the stone column divided by shear strain in the surrounding soil.

To demonstrate the wide variation among the predictions of the aforementioned methods, each equation is applied to a generic case study where deposits of silty sand are improved by stone columns. The data is taken from an actual site in Abu Dhabi. The area replacement ratio, A_r =11%, angle of friction, $\varphi_{col.} = 38^0$ and shear modulus ratio, G_r = 8. As expected, the flexural beam assumption in Eq. 4 gives greater K_G value (89%) than the shear compatibility (55%), and the area ratio (72%) approaches. The shear strain compatibility predicts

almost 4 times the reduction in liquefaction susceptibility predicted by the flexural beam theory and 2 times that predicted by the area ratio approach.

However, the K_G value predicted by Rayamajhi et al. [11] (91%) is counterintuitively higher than that predicted by Gonghour and Pestana [9] as shown in Fig. 1. Eq. 8 produces a conservative value for the shear strain and then a single value for K_G is estimated for the entire soil depth. The comparison clearly indicates that a reasonable K_G estimation has to come from a more realistic distribution of shear strains which captures the variation along the depth and not a single value. This requires advanced numerical simulation of the dynamic load to predict realistic strains. Then, using Eq. 7, the distribution of K_G over soil depth can be determined. The average of this distribution can be lower than the conservative assumption used in this demonstration.

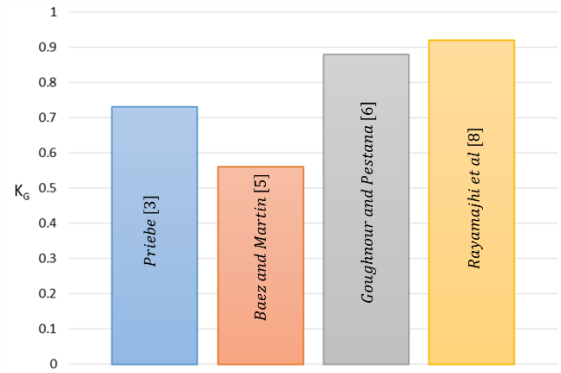

Fig.1 Comparison between different methods of estimating K_G value

3. STATIC ANALYSIS

Plate load tests on stone columns are common in project specifications to ensure that the columns are constructed with sufficient strength and stiffness. The Young's modulus is best back analyzed from the slope of the unloading portion of the load settlement curves [16], which better reflects the stone column's elastic behavior. Therefore, the Young's modulus can be calculated using Eq. 9 as recommended by the British Standards [17]. The plate load test can be numerically replicated in an axisymmetric finite element model. Fig. 2 compares between numerical predictions and field measurements from the Tanna coal development project [16]. The figure shows that the numerical model captures well the unload reload portion of the load settlement curve from which the interpreted stiffness is calculated using Eq. 9.

$$E_{int} = \frac{\Delta q}{\Delta s}(1-\nu^2)b\frac{\pi}{4} \quad (9)$$

In Eq. 9, E_{int} is the interpreted Young's modulus, Δq is the selected range of applied contact pressure considered, Δs is the change in total settlement for the corresponding change in the applied contact pressure Δq, ν is the Poisson's ratio, and b is the diameter of the plate.

The numerical simulation also gives an insight into the significance of the interpreted Young's modulus, E_{int}. In the Tanna case study, E_{int} is estimated by 200 MPa, while the Young's modulus used as an input parameter in the analysis is 725 MPa which lead to a good match with field measurements. There is a ratio of 0.276 between interpreted and actual stone column stiffness due to the effect of surrounding soil stiffness and column material strength on field test results.

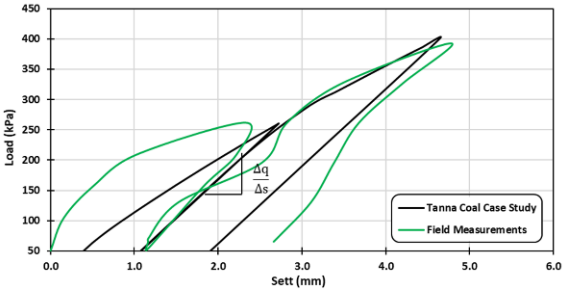

Fig.2 A comparison between numerical predictions of the Tanna coal case study and field measurements

The relationship between interpreted and actual stone column stiffness is best investigated by a parametric study using a prototype case. Fig.3a shows the dimensions and boundary conditions of the prototype model, in the two-dimensional finite element software Plaxis 2D. The lateral boundaries are fixed in the horizontal direction, while the bottom boundary is fixed in the vertical and horizontal directions. Stone column solid elements and surrounding soil elements are connected at their nodes with no interface elements employed. The vibro-replacement causes significant interconnection between the stones and the surrounding soil which leads to compatible deformations. All soil materials are modeled using the Mohr-Coulomb constitutive model. The material properties are chosen for typical sand and stone column material, as shown in Table 1. The model consists of a 10-m-thick loose silty sand layer, and the groundwater is at 2 meters from the ground surface. This silty sand layer has an average N_{SPT} corrected number of blows count ($N1_{60}$) = 14 which means the relative density (D_r) value is 55% [18]. Stone columns are 1.0 m in diameter, which extend to the bottom of the liquefiable layer with an assumed spacing 3m center to center (3D), and the area replacement ratio A_r (A_c /A) is 1/9 ≈ 11%. In the parametric study, the ratio between the stone column's stiffness and surrounding soil stiffness, E_{col}/E_{soil}, is taken as 2, 4, 8, and 15; and the stone column friction angle, $\varphi_{col.}$ = 38°, 40°, and 42°. The

stages of analysis represent a plate load test as given in the ASTM D1194 procedure [19]. In each simulation, a surface load is applied to the top of the stone column and increased until enough plastic points develop. Then, the load is removed and the slope of the unloading load-displacement path is determined.

Fig. 3b shows the values of E_{int} from the numerical simulation for each value of E_{col} entered as an input parameter. The trends do not vary significantly with changing the friction angle of the column material. The same trend is observed such that for low values of E_{col} (E_{col} is not that low in typical applications), E_{int} is close to the input value. However, at high E_{col}, the E_{int} can become approximately 20% of the input value. The friction angle effect tends to diminish at extreme E_{col} values (i.e., lower than 50 MPa, or higher than 175 MPa) and has more significant effect when E_{col} is intermediate.

Table 1 Input parameters for the Mohr Coulomb soil model used in static analysis

Parameter	Sand	Stone Columns
Unit Weight, γ (kN/ m^3)	16	21
Friction Angle, ϕ^o	28	varies
Dilation Angle, ψ^o	0	8
Young's Modulus, E (kPa)	13000	varies
Poisson's Ratio	0.3	0.2

4. DYNAMIC ANALYSIS

Numerical models can also demonstrate the effect of stone columns on improving liquefaction resistance if a suitable material model is used. To the best of the authors' knowledge, the two most cited dynamic constitutive models recently are: UBC3D-PLM and PM4Sand. The PM4Sand model is an elastoplastic one, limited to 2-D definitions of stress. It performs non-linear seismic deformation analysis to estimate the soil's stress-strain behavior, calculate induced pore pressures, and predict post-liquefaction ground deformations during earthquakes. The model follows the basic framework of bounding surface plasticity, which is compatible with critical state soil mechanics in sands [20]. However, PM4Sand adds to the Dafalias-Manzari framework such that the model calibration is linked to dynamic soil behavior observed in experiments or using case history-based design correlations [21]. This framework determines volumetric behavior (contractive or dilative) based on the current state of stresses and the soil's density status, as shown in Fig. 4. In this framework, the soil behavior is determined by the locations of the bounding surface, dilatancy surface, and critical state surface using stress ratios, M_b, M_d, and M_c, which depend on the relative state index, ξ_R. As shown in the figure, the values of M_b and Md are significantly different if the soil is looser or denser than the critical state.

The PM4Sand input parameters are related to the data typically available in geotechnical engineering practice such as SPT readings, CPT readings, and shear wave velocities. Such parameters are the apparent relative density, D_r which along with the maximum and minimum void ratios, control the peak drained and undrained strengths, volumetric behavior, and rate of strain accumulation.

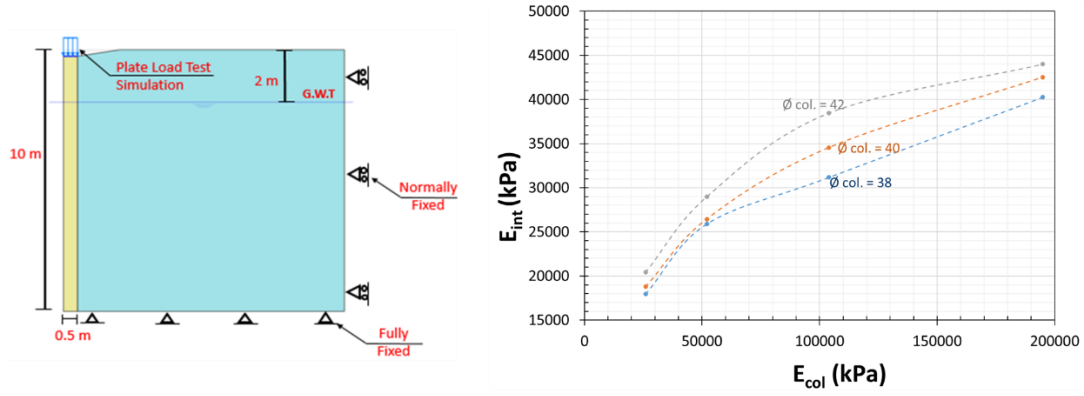

(a) (b)

Fig. 3 Model and results of static analysis; a) axisymmetric model, and b) relationship between interpreted and actual stone column stiffness as predicted numerically

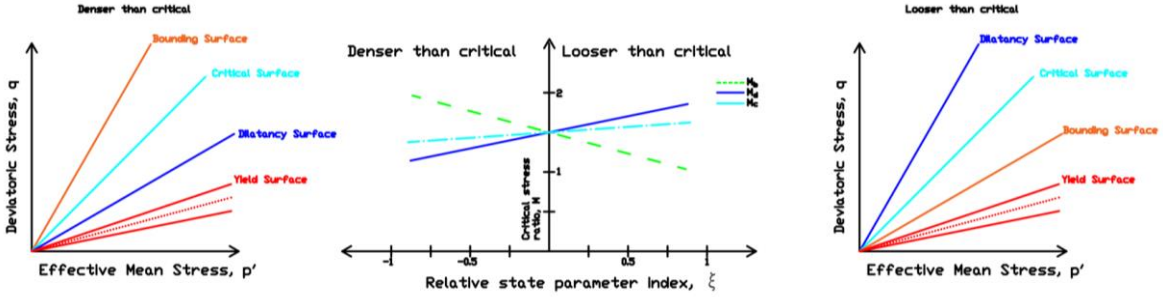

Fig. 4 Schematic of the yield, critical, dilatancy, bounding lines of the PM4Sand in q-p space

Parameters also include the shear modulus coefficient, G_0, which controls the small strain behavior. The model predicts dilatancy using Q and R parameters defined by Bolton's dilatancy relationship [22]. Furthermore, the calibration determines the value of a contraction rate parameter, h_{po}, which adjusts the behavior to specific values of cyclic resistance ratio (CRR) based on cyclic lab tests. Correlations of the primary parameters with the standard penetration test ($N1_{60}$) are provided, as shown in Eqs. 10-12.

$$D_R = \sqrt{\frac{N1_{60}}{C_d}} \tag{10}$$

$$G_0 = 167\sqrt{N1_{60} + 2.5} \tag{11}$$

$$G_{max} = G_0 p_A \sqrt{\frac{p}{p_A}} \tag{12}$$

In the equations above, p_A is the atmospheric pressure, p is the mean effective stress, ($N1_{60}$) is the corrected SPT value, and C_d = 46 [23].

The UBC3D-PLM is a constitutive model that provides a simple approach to determine the onset of the liquefaction phenomenon in sandy and non-plastic silty soils due to an earthquake. The model is a 3-D generalized formulation of the original 2D UBCSAND model [24]. It is an elastoplastic model that utilizes isotropic and simplified kinematic hardening rules for primary and secondary yield surfaces shown in Fig. 5 to consider the effect of soil densification and predict a smooth transition into the liquefied state during undrained cyclic loading [25].

The primary yield surface is based on isotropic hardening and is activated when the mobilized friction angle, φ'_{mob} reaches the maximum value of a mobilized friction angle that the soil has ever experienced, $\varphi'_{mob,max}$. Otherwise, the behavior is controlled by the secondary yield surface (φ'_{mob}). The mobilized friction angle is not allowed to surpass an input value for the peak friction angle, φ'_p. Both surfaces expand during loading, while the secondary surface contracts during unloading to allow for elastic behavior. Then, the surface expands again to enable elastoplastic behavior as soon as the soil is reloaded.

The model flow rule is based on the stress-dilatancy theory [26]. This model properly captures the evolution of the excess pore pressures in the sandy soils and the onset of liquefaction in undrained loading conditions. Post liquefaction behavior of loose non-cohesive soils and cyclic mobility of dense non-cohesive sands require a stiffness degradation rule. The model input parameters are correlated to the standard penetration field test corrected number of blows [27] as seen in Eqs. 13-15.

$$k_B^e = 0.7 \times k_G^e \tag{13}$$

$$k_G^e = 21.7 \times 20 \times (N1_{60})^{0.333} \tag{14}$$

$$k_G^p = k_G^e \times (N1_{60})^2 \times 0.003 + 100 \tag{15}$$

The stiffness parameters mentioned in the above equations are: k_B^e is the elastic bulk modulus factor, k_G^e is the elastic shear modulus factor, k_G^p is the plastic shear modulus factor. The rate stress dependency parameters are m_e for the elastic bulk modulus, n_e for the elastic shear modulus, and n_p for the plastic shear modulus; while p_{ref} is the reference pressure.

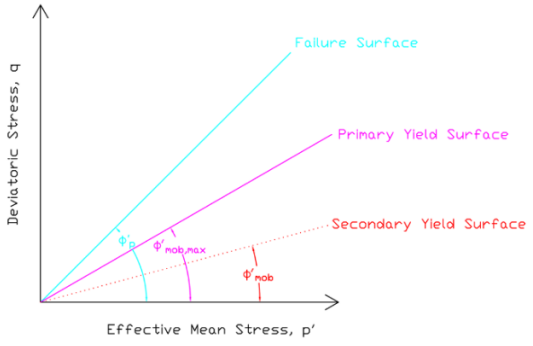

Fig.5 UBC3D-PLM primary, secondary yield and failure surfaces

The numerical investigation is performed using two-dimensional finite element software Plaxis 2D modeling a plane-strain problem. The earthquake

used in the analysis is the Oakland 1989 earthquake with 0.3 g peak ground acceleration and a magnitude, M_w = 6.93. The boundary conditions tie the displacements of nodes on the left and right sides at the same elevation together (Tied-degree of freedom) with 1-D wave propagation analyses. The excitation applied at the soil deposit base is an acceleration history in the horizontal direction only and the base below is considered as a compliant base.

The analyses involve an unimproved sandy soil profile behavior under a reference earthquake time history that leads to soil liquefaction in the free-field condition. Then, the improved case is modeled using a triangular pattern of stone columns. The unit cell is simulated in the 2D plane strain model using an alternative geometrical transformation approach [28]. This method is based on the equivalence of the column drainage capacity in the axisymmetric and plane-strain cases. The method gives the equivalent column width in a horizontal direction while using similar stiffness and shear strength parameters. The relationship in Eq. 16 gives the plane-strain column width based on the equivalence of area replacement ratio.

$$b_c = B \times \frac{r_c^2}{R^2} \quad (16)$$

In the equation above b_c is the equivalent stone column radius, and B is the unit cell radius in plane-strain conditions. The axisymmetric radii are r_c for the stone column and R for the unit cell.

This equation gives $b_c \approx 0.15$ m, B ≈ 1.3 m to represent the column diameter 1m, and the 3m unit cell width, as shown in Fig. 6. In the figure, there are two points to consider in the analysis; a point at the stone column's perimeter (point 1) and another at the unit cell perimeter (point 2). The area around point 1 is quickly drained, and hence, minimum pore water pressure is generated there. Point 2 exhibits the maximum pore water pressure because it is furthest from any stone column. Therefore, the estimations of liquefaction improvement consider values at point 2 throughout the depth of the soil.

The two previously described dynamic constitutive models (i.e., PM4Sand and UBC-3D PLM) represent the sandy soil material with the input parameters listed in Tables 2 and 3. The stone column material is represented by the UBC3D-PLM constitutive model in both simulations. The stone column is also considered completely drained to eliminate the excess pore water pressure calculation because of its large drainage capacity, which produces approximately zero excess pore water pressure. Also, this condition decreases the calculation time without compromising the accuracy of results. This analysis does not consider the effect of construction on densifying the surrounding soil. The PM4Sand parameters are calibrated for this analysis using the SPT-based empirical correlations that relate SPT values to the cyclic resistance ratio (CRR) of soils at vertical stress equivalent to the atmospheric pressure [29]. However, because this is a prototype simulation and there is no cyclic laboratory data available, the cyclic direct simple shear (CDSS) test tool in Plaxis is used to calibrate the contraction rate parameter (h_{po}) as per literature recommendation [21].

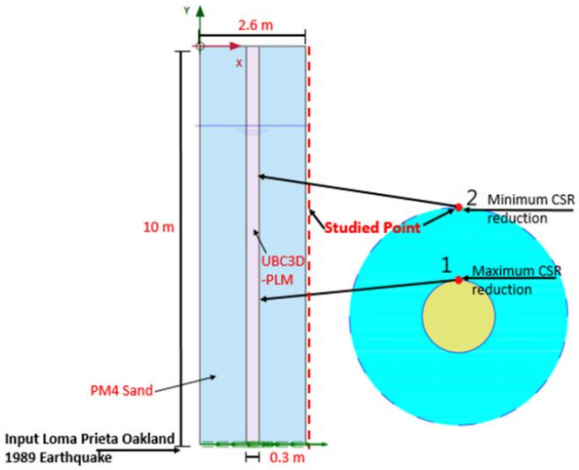

Fig. 6 Dimensions and boundary conditions of the plane strain finite element model used in dynamic analysis

The effect of stone column stiffness is investigated by considering E_{col}/E_{soil} as 2, 4, 8, and 15. The lower values in this range are not realistic and only chosen to check the problem sensitivity to the parameters. Fig. 7 shows the maximum normalized change in pore water pressure ($r_{u,max}$) at point (2) for each condition achieved at the end of earthquake application. The maximum normalized pore water pressure ($r_{u,max}$) is calculated by finding the maximum value of the effective vertical stress change during the analysis divided by the initial effective overburden at each depth. If the maximum pore water pressure ratio exceeds the 0.7 value, the soil element at this value is considered in a liquefied state [30]. The figure presents the improved and unimproved cases using both the PM4Sand and UBC3D-PLM models. In the unimproved case, the UBC3D-PLM model predicts an almost constant $r_{u,max}$ value with depth indicating a complete loss of strength over the whole model. The model predicts significant improvement due to stone column construction (lower $r_{u,max}$ values); however, this improvement seems to slightly decrease with increasing E_{col}/E_{soil} ratio, which is counterintuitive. On the other hand, PM4Sand model predictions seem more realistic, as they show reasonable effects of depth (higher effective stress changes closer to the bottom boundary), and of stone column stiffness ($r_{u,max}$ decreases with increasing E_{col}/E_{soil}).

Table 2 Input parameters for the PM4Sand soil model used in dynamic analysis

Parameter	Sand
Unit Weight, γ (kN/ m^3)	16
Relative Density, D_{ro} (%)	55
Shear Modulus Coefficient, G_o (dimensionless)	678.4
Contraction Rate Prameter, h_{po} (dimensionless)	0.56
Bounding Surface Prameter, n_b (dimensionless)	0.5
Dilatancy Surface Parameter, n_d (dimensionless)	0.1
Poisson's ratio	0.3
Critical State Friction Angle, ϕ_{cv}	33°
Critical State Line Parameters (dimensionless), Q and R	10 and 1.5

The UBC3D-PLM is a reputable model that has been successfully used to capture earthquake deformations, as several researchers showed for the Kobe port earthquake [31]. However, the numerical simulation of such an earthquake involves large strains and number of cycles. When low shear strains prevail, due to the reinforcement from the stone column, UBC3D-PLM calculates no accumulated shear strains during an earthquake because the hysteresis loop repeats with no additional growth in the cyclic strain amplitude after a certain number of cycles [32, 33]. Hence, the PM4Sand is considered more suitable for analyzing stone column effects on liquefaction resistance. Fig. 8 shows PM4Sand predictions of $r_{u,max}$ using φ_{col} = 38^0, 40^0, and 42^0. As the stiffness ratio (E_{col}/E_{soil}) increases, the effect of stone column friction angle becomes less significant.

Instead of calculating the shear stress reduction factor (K_G) from shear strains, it is derived from the distribution of pore water pressure ratio (r_u) in this analysis. First, the factor of safety (F.S.) is calculated from r_u following [34]. Then, K_G is considered the F.S. ratio between the unimproved and improved cases. Fig. 9 shows the effect of stone column stiffness and friction angle on numerically predicted K_G values. For low stiffness values, friction angle effect is more apparent. As column stiffness increases, K_G values decrease as expected but friction angle effect diminishes. The results also indicate that K_G decreases linearly from ground surface down to half of the layer thickness, then keeps constant till the end of the layer.

Fig. 10 compares between the numerically predicted K_G values and the previously discussed semi analytical equations. The analyses show how the gap between the different methods increase with increasing column stiffness. The numerical predictions agree well with the flexural deformation [9] and the combined [11] approaches. On the other hand, the shear strain compatibility [8] and the area ratio [5] approaches overestimate the reduction in shear stresses. The figure also indicates that an average K_G value from the shown distribution is significantly less than the conservative value calculated from design formula from [11].

Table 3 Input parameters for the UBC-3DPLM soil model used in dynamic analysis

Parameter	Sand	Stone Columns
Unit Weight, γ (kN/ m^3)	16	21
Bulk Modulus Ratio, K_B^e (dimensionless)	736.6	Varies
Shear Modulus Ratio, K_G^e (dimensionless)	1052	Varies
Plastic Shear Modulus Ratio, K_G^e (dimensionless)	741.5	Varies
Peak friction angle, ϕ_p	28°	Varies
Critical state friction angle, ϕ_{cv}	28°	33°
$N1_{60}$	14	-
m_e	0.5	0.5
n_e	0.5	0.5
n_p	0.4	0.4

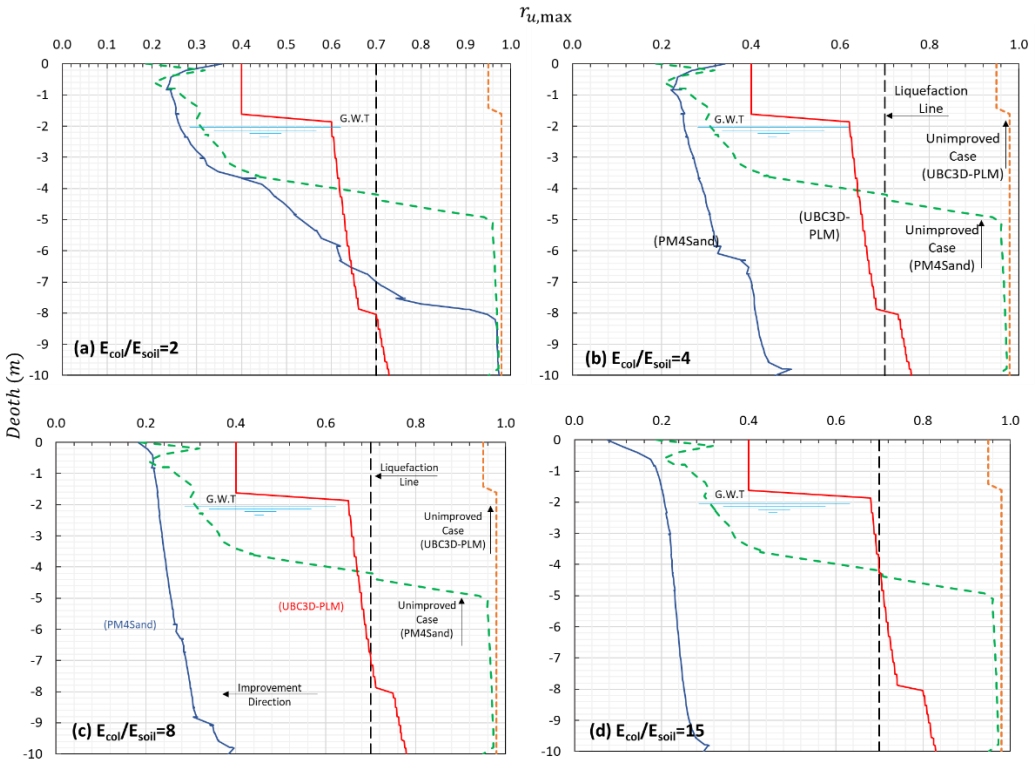

Fig. 7 Maximum normalized change in pore pressure ($r_{u,max}$) as predicted by PM4Sand vs UBC3D-PLM models for φ_{col} = 380 with values of E_{col} / E_{soil}= a) 2, b) 4, c) 8, d) 15

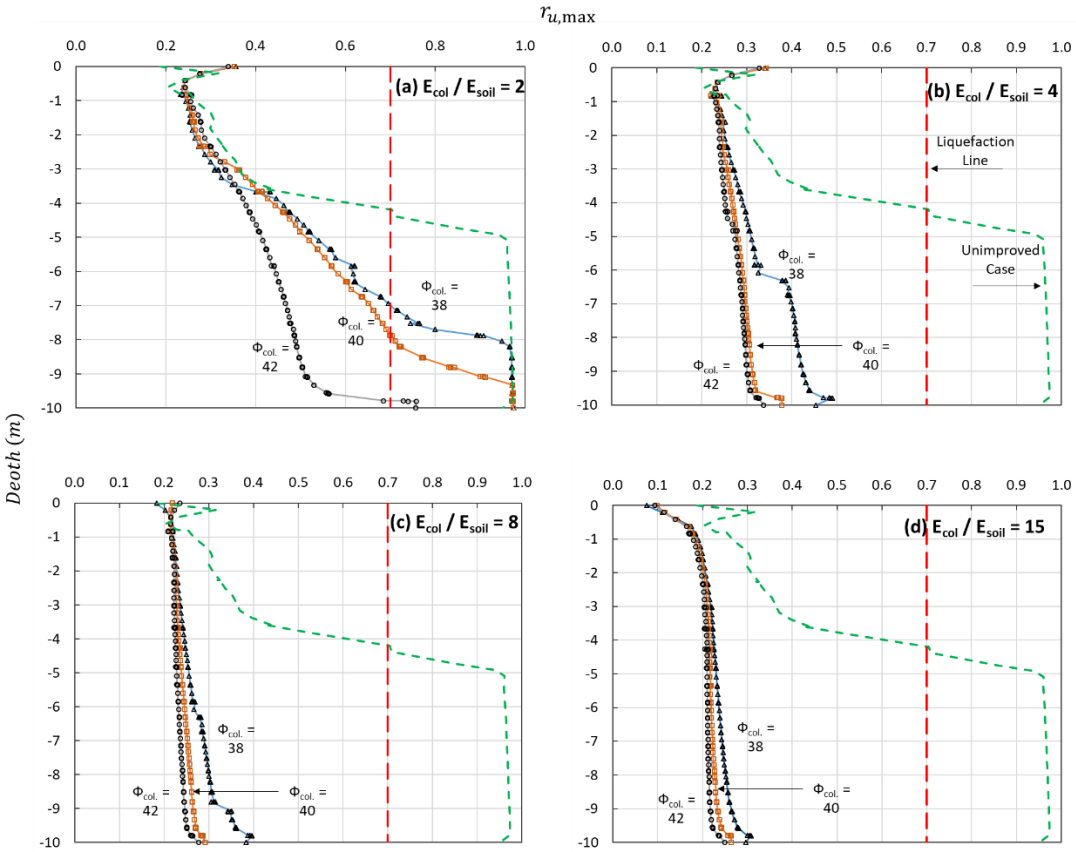

Fig. 8 Maximum normalized change in pore pressure ($r_{u,max}$) for φ_{col} = 38^0, 40^0, and 42^0 with values of E_{col} / E_{soil}= a) 2, b) 4, c) 8, d) 15

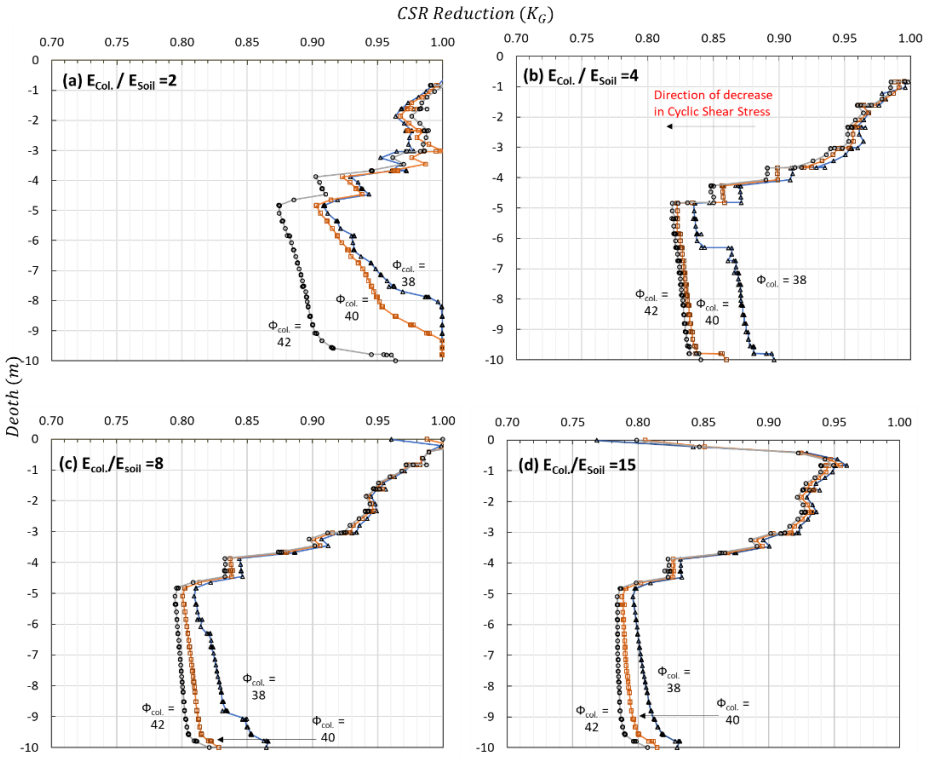

Fig. 9 Distribution of cyclic shear stress reduction factor, K_G with depth for E_{col}/E_{soil} = a) 2, b) 4, c) 8, d) 15

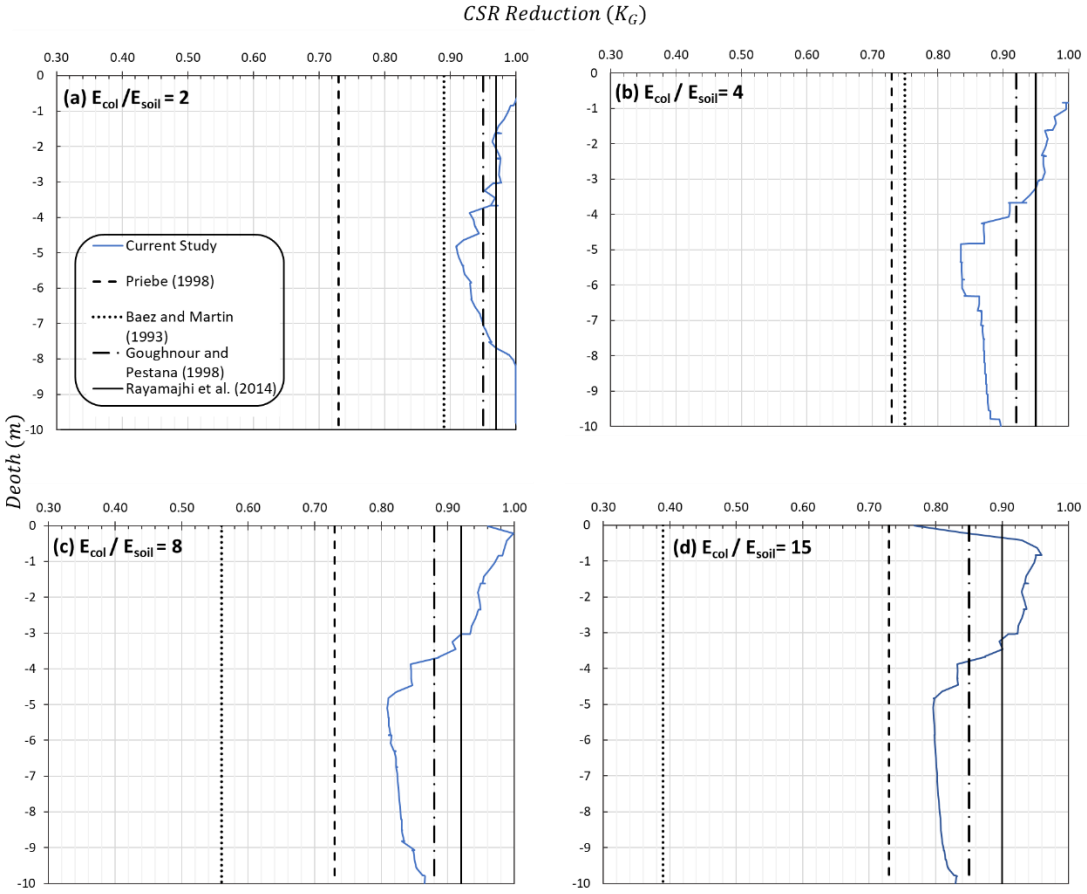

Fig. 10 Comparison between K_G values from dynamic analyses and design formulas from literature for φ_{col} = 38^0 stone columns with E_{col} / E_{soil} = a) 2, b) 4, c) 8, d) 15

5. DESIGN CURVE

The relationship between interpreted and actual stone column stiffness and that between actual column stiffness and shear stress reduction can be combined as shown in Fig. 11. The figure shows a quality control curve from which the interpreted stiffness, from a plate load test for example, can give a preliminary estimation of K_G value. Results from the static analysis are normalized by the soil stiffness (horizontal axis), and column stiffness (vertical axis). Hence, using the figure requires an initial assumption for the E_{int}/E_{col} ratio. For example, if E_{int} = 40 MPa, and average E_{soil} = 15 MPa; an assumed E_{col} = 80 MPa leads to a point (5.333, 0.5) which is outside the curve. An assumed E_{col} = 165 MPa leads to a point (11, 0.24) which falls on the curve. Average K_G values from the dynamic analysis are used to create the upper part from the curve. In the previous example, the 165 MPa columns decreases shear stresses in the 15 MPa soils by 0.855 on average.

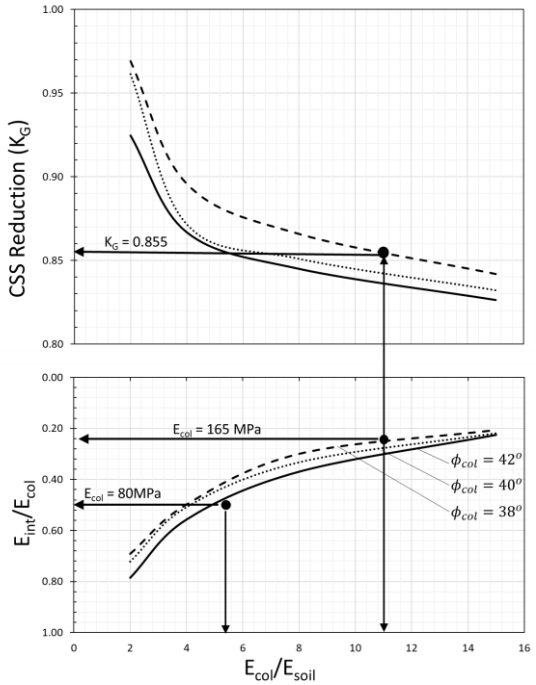

Fig. 11 Quality control design curves relating interpreted stone column stiffness ($E_{int.}$) to the cyclic shear stress ratio reduction factor (K_G)

The applicability of this curve is limited to stone columns in silty sand soils and not clayey soils for example. However, it applicability is not affected by a change in penetration depth in the static analysis or in area ratio in the dynamic analysis from the prototype assumptions. The effect of stone column penetration depth to the soil deposit depth ratio (L/H) is checked by trying L/H = 0.5, 0.7, and 1 for stone columns with the friction angle $\varphi'col=40^0$. Results show that variation in interpreted stiffness values is within 3%. Deformation contours indicate a bulge depth of 2.5 times the column diameter which agrees with literature [6]. As long as the column extends beyond the bulge depth, the change in interpreted stiffness is not significant.

The second variation is to check the effect of area replacement ratio (A_r) on K_G. The new A_r = 25% but the rest of the analysis components and material properties remain the same. The simulation results generally show no significant differences in r_u values (which ultimately leads to no variation in K_G) with the increased area replacement ratio value. Hence, stone columns area ratio stiffening effect is only within 5%, as long as the relative permeability does not change.

6. CONCLUSIONS

This paper describes an investigation into the effect of stone column on reducing liquefaction potential of silty sands and how can this be indicated by quality control tests in the field. The paper presents a design aid curve to relate the stone column stiffness (E_{col}) deduced from plate load testing (static analysis) and the reduction factor, K_G, in shear stresses (dynamic analysis). This curve helps field engineers make a quick estimate of enhancement in liquefaction resistance from plate load testing in standard quality control programs. The relationship uses two different groups of numerical simulations. First, a series of plate load test simulations using an axisymmetric numerical model interprets the stone column's stiffness (E_{int}) from load-settlement curves. Second, a series of dynamic analyses of a unit cell subjected to earthquake loading considering improved and unimproved conditions. The two groups of simulations consider the effect of variations in the column's stiffness and angle of friction. The following conclusions can be drawn from the two groups of analyses:

a. Popular methods to estimate reduction in liquefaction potential by constructing stone columns give greatly varying estimates. All the methods require the knowledge of actual column stiffness in the field.
b. In a static simulation of the plate load test, the E_{int}/E_{col} decreases significantly with the increase in column stiffness. The value of E_{int} can be in the order of only 20% of the column stiffness. For extreme column stiffness values (lower than 50 MPa and higher than 175 MPa), the friction angle value has little significance. The effect of friction angle increases when column stiffness values are intermediate.

c. The use of plane strain models and approximation methods for the stone column dimensions in dynamic analysis enables simple numerical models to estimate stress reduction factors. Numerical predictions agree with the methods from literature that use the combined shear and flexural deformation approach. In such models, stress reduction factors can be calculated using changes in pore pressures rather than distributions of shear strains.
d. The PM4Sand material model is more suited to show changes in shear stresses due to constructing stone columns than the UBC3D-PLM material model. Hence, analysis using PM4Sand gives reasonable estimates of enhancement in liquefaction resistance. On the other hand, the UBC3D-PLM overestimates the pore water pressure ratio and projects the same accumulation of shear strains with and without the stiff stone columns.
e. The design aid curve presented herein is suitable for the whole range of typical area ratios and stone column penetration depths. As long as the stone column penetrates the soil to depths beyond the typical bulge range (2-3D), the curve gives a reasonable estimation of the column stiffness.

7. REFERENCES

[1] Bouassida M., and Klai M., Challenges and improvement solutions of Tunis soft clay, International Journal of GEOMATE, Vol. 3, Issue 1, 2012, pp. 296-305.

[2] Quispe I.F.S., Tito J.C., and Apaza M.E., Stability Analysis for an Airport Embankment, Evaluating Short and Long Term Techniques, International Journal of GEOMATE, Vol. 14 Issue 45, 2018, pp.103-108.

[3] Fattah M.Y., and Majeed Q.G., A study on the behaviour of geogrid encased capped stone columns by the finite element method, International Journal of GEOMATE, Vol. 3, Issue 1, 2012, pp. 343-50.

[4] Wang G., Wei X. and Liu H., Liquefaction evaluation of dam foundation soils considering overlying structure, Journal of Rock Mechanics and Geotechnical Engineering, Vol. 7, Issue 2, 2015, pp. 226-232.

[5] Priebe H.J., Vibro replacement to prevent earthquake induced liquefaction, Ground engineering, Vol. 31, Issue 9, 1998, pp. 30-33.

[6] Barksdale R.D., and Bachus, R.C., Design and Construction of Stone Columns Volume I Federal Highway Administration Report FHWA, RD-83/026, National Technical Information Service, Springfield, Virginia, 1983.

[7] Bahadori H., Farzalizadeh R., Barghi A., and Hasheminezhad A., A comparative study between gravel and rubber drainage columns for mitigation of liquefaction hazards, Journal of Rock Mechanics and Geotechnical Engineering, Vol. 10, Issue 5, 2018, pp. 924-934.

[8] Baez J.I., and Martin, G.R., Advances in the design of vibro systems for the improvement of liquefaction resistance, Proceedings of the Symposium on Ground Improvement, Canadian Geotechnical Society, Vancouver, 1993, pp. 1-16.

[9] Goughnour R.R., and Pestana J.M., Mechanical behavior of stone columns under seismic loading, Proceedings of the 2nd International conference on Ground Imporvement Techniques, Singapore, 1998, pp.157-162.

[10] Olgun C.G., and Martin II J.R., Numerical modeling of the seismic response of columnar reinforced ground, Geotechnical earthquake engineering and soil dynamics IV, GSP 181, Reston, VA, 2008.

[11] Rayamajhi D., Nguyen T.V., Ashford S.A., Boulanger R.W., Lu J., Elgamal A., and Shao L., Numerical study of shear stress distribution for discrete columns in liquefiable soils, Journal of Geotechnical and Geoenvironmental Engineering, Vol 140, Issue3, 2014, p. 04013034.

[12] Seed H.B., and Idriss I.M., Simplified procedure for evaluating soil liquefaction potential, Journal of the Soil Mechanics and Foundations division, Vol. 97, Issue 9, 1971, pp. 1249-1273.

[13] Green R.A., Olgun C.G., and Wissmann K.J., Shear stress redistribution as a mechanism to mitigate the risk of liquefaction, Geotechnical earthquake engineering and soil dynamics IV, GSP 181, Reston, VA, 2008.

[14] Olgun C.G., and Martin II J.R., Seismic Behavior of Columnar Reinforced Ground, Proceedings of 14th World Conference on Earthquake Engineering, Beijing, China, 2008.

[15] Rayamajhi D., Ashford S.A., Boulanger R.W., and Elgamal A., Dense granular columns in liquefiable ground. I: shear reinforcement and cyclic stress ratio reduction, Journal of Geotechnical and Geoenvironmental Engineering, Vol. 142, Issue 7, 2016, p.04016023.

[16] Fatahi B., Basack S., Premananda S., and Khabbaz H., Settlement prediction and back analysis of Young's modulus and dilation angle of stone columns, Australian Journal of Civil Engineering, Vol. 10, Issue 1, 2012, pp.67-79.

[17] BS EN 1997-2, Eurocode 7 Geotechnical Design–Part 2, Ground investigation and testing, BSI, London, UK, 2007.

[18] Idriss I.M., and Boulanger R.W., Semi-empirical procedures for evaluating liquefaction potential during earthquakes, Soil dynamics and earthquake engineering, Vol. 26, Issue 2-4, 2006, pp. 115-130.
[19] ASTM D 1194-94, Standard test method for bearing capacity of soil for static load and spread footings, 2003.
[20] Dafalias Y.F., Manzari, M.T., Simple plasticity sand model accounting for fabric change effects, Journal of Engineering Mechanics, Vol. 130, Issue 6, 2004, pp.622–634.
[21] Boulanger R.W., and Ziotopoulou K., PM4Sand (Version 3): A sand plasticity model for earthquake engineering applications, Report No. UCD/CGM-15/01, Center for Geotechnical Modeling, Department of Civil and Environmental Engineering, University of California, Davis, California, 2015.
[22] Bolton M.D., The strength and dilatancy of sands, Geotechnique,Vol. 36, Issue 1, 1986, pp. 65-78.
[23] Idriss I.M., and Boulanger R.W., Soil liquefaction during earthquakes, Report No. MNO-12, Earthquake Engineering Research Institute, Oakland, CA, USA, 2008.
[24] Puebla H., Byrne M., and Phillips, P., "Analysis of canlex liquefaction embankments prototype and centrifuge models." Canadian Geotechnical Journal, 34 (pp. 641–657) 1997.
[25] Petalas A., and Galavi V., Plaxis Liquefaction Model UBC3D-PLM, Plaxis B.V, Delft, The Netherlands, 2013.
[26] Rowe P.W., The stress-dilatancy relation for static equilibrium of an assembly of particles in contact, Proceedings of the Royal Society of London, Series A, Mathematical and Physical Sciences, Vol. 269, Issue 1339, 1962, pp. 500-527.
[27] Makra A., Evaluation of the UBC3D-PLM constitutive model for prediction of earthquake induced liquefaction on embankment dams, M.Sc. Thesis, TU Delft, The Netherlands, 2013.
[28] Tan S.A., Tjahyono S., and Oo K.K., Simplified plane-strain modeling of stone-column reinforced ground, Journal of Geotechnical and Geoenvironmental Engineering, Vol. 134, Issue 2, 2008, pp. 185-194.
[29] Idriss I.M., and Boulanger R.W., SPT-based liquefaction triggering procedures, Report no. UCD/CGM-10/2, Center for Geotechnical Modeling, University of California, Davis, CA, 2010.
[30] Laera A., and Brinkgreve R.B.J., Site response analysis and liquefaction evaluation. Plaxis Knowledge Base, 2015.
[31] Inagaki H., Iai S., Sugano T., Yamazaki H. and Inatomi T., Performance of caisson type quay walls at Kobe port, Soils and foundations, Vol. 36, 1996, pp.119-136.
[32] Carey T.J., and Kutter B.L., Comparison of Liquefaction Constitutive Models for a Hypothetical Sand, Geotechnical Frontiers 2017 : Seismic Performance and Liquefaction, GSP 281, 2017.
[33] Demir S. and Özener P., Comparison of Seismic Performance of High Modulus Columns in Liquefiable Soils, In Geotechnical Earthquake Engineering and Soil Dynamics V: Liquefaction Triggering, Consequences, and Mitigation, American Society of Civil Engineers, Reston, VA, 2018, pp. 160-169.
[34] Tokimatsu K., and Yoshimi Y., Liquefaction of sand due to multidirectional cyclic shear, Soils and foundations, Vol. 22, Issue 3, 1982, pp.126-130.